Oxygen mediated phase transformation in room temperature grown TiO_2 thin films with enhanced photocatalytic activity

D. Banerjee, A. Barman, S. Deshmukh, C. P. Saini, G. Maity, S. K. Pradhan, M. Gupta, D. M. Phase, S. S. Roy, and A. Kanjilal

Citation: Appl. Phys. Lett. **113**, 084103 (2018); doi: 10.1063/1.5040916
View online: https://doi.org/10.1063/1.5040916
View Table of Contents: http://aip.scitation.org/toc/apl/113/8
Published by the American Institute of Physics

Oxygen mediated phase transformation in room temperature grown TiO_2 thin films with enhanced photocatalytic activity

D. Banerjee,[1] A. Barman,[1] S. Deshmukh,[1] C. P. Saini,[1,2] G. Maity,[3] S. K. Pradhan,[3] M. Gupta,[4] D. M. Phase,[4] S. S. Roy,[1] and A. Kanjilal[1,a)]
[1]*Department of Physics, School of Natural Sciences, Shiv Nadar University, NH-91, Dadri, Gautam Buddha Nagar, Uttar Pradesh 201 314, India*
[2]*Inter-University Accelerator Centre, Aruna Asaf Ali Marg, New Delhi 110 067, India*
[3]*Department of Physics, The University of Burdwan, Golapbag, Burdwan 713104, West Bengal, India*
[4]*UGC-DAE consortium for Scientific Research, Khandwa Road, Indore, Madhya Pradesh 452001, India*

(Received 22 May 2018; accepted 27 July 2018; published online 22 August 2018)

Room temperature transformation from anatase (A-TiO_2) to rutile (R-TiO_2) thin films through an intermediate mixed phase on stainless steel driven by a controlled oxygen flow rate (OFR) is investigated. Such OFR dependent phase transition is confirmed by X-ray diffraction and also consistent with X-ray absorption spectroscopy at Ti L and O K-edges, showing a long range ordering in TiO_6 octahedral symmetry. X-ray photoelectron spectroscopy reveals a gradual reduction in Ti_2O_3 and/or TiO intermediate phases with increasing OFR. Finally, an enhanced photocatalytic activity is observed in the mixed phase and discussed in terms of photo-generated charge transport in the type-II staggered band structure between A-TiO_2 and R-TiO_2 phases. *Published by AIP Publishing.*
https://doi.org/10.1063/1.5040916

Engineering the crystallinity and bandgap of metal oxides has phenomenological importance owing to their several applications in optoelectronics, sensing, memory devices, photocatalysis, etc.[1–3] Among many transition metal oxides, TiO_2 has attracted attention not only for its non-toxicity[4] and high temperature stability[5] but also for its ability to generate stable electron-hole pairs and thus suitable for degrading organic pollutants[6] and hydrogen generation via water splitting.[4] An ideal photocatalyst requires matching of the conduction band with the redox-potential of water for generating oxidative oxygen species ($\cdot OH$, $\cdot O_2^-$) which degrade the organic pollutants. In this respect, the structure and chemical states of TiO_2 play a decisive role in band-gap modification.[7] For instance, photocatalytic performance of TiO_2 is highly reliant on its thermodynamically stable rutile or metastable anatase phase. However, high temperature annealing is a prerequisite for achieving such crystalline phases.[8,9] It is to mention that the rutile has less bandgap (~3 eV) with respect to anatase (~3.2 eV).[10] Such a high bandgap hinders its performance under the visible spectrum. Therefore, it is important to tune the bandgap and crystallinity of TiO_2 to enhance its performance as a photocatalyst as well as for photovoltaic and optoelectronic applications. These can be achieved by the introduction of sub-bandgap states either by doping foreign elements[11] or self-doping, i.e., introduction of Ti^{3+} or oxygen vacancies (OVs).[12] These Ti^{3+} and OVs can introduce isolated defect states near the conduction band minima which minimize the effective bandgap. The bandgap reduction has been demonstrated earlier by engineering the high temperature annealing induced generation of OVs.[13] Ion-irradiation induced bandgap tuning of TiO_2 has also been demonstrated and discussed in the light of Ti^{3+} and OV induced formation of defect states.[14] However, the enhancement in photocatalysis response by formation of such defect induced sub-bandgap states in TiO_2 is uncertain. In this context, a suitable ratio of anatase and rutile phases in mixed-phase TiO_2 exhibits a relatively high photocatalytic performance owing to efficient inter-granular charge transfer,[15] though it requires high temperature annealing to maximize the performance and thus leads to an increase in the thermal budget. In the case of TiO_2 films, a high temperature treatment can also introduce undesired diffusion of impurities from the underneath low melting point and chemically reactive substrate and thus hinders the photocatalytic performance. Therefore, it requires a facile and cost effective approach where the mixed-phase of TiO_2 films with enhanced photocatalytic activity can be achieved at room temperature (RT). In fact, the desired phase evolution in TiO_2 at RT with varying oxygen flow rates (OFR) during deposition has not been explored yet and hence their catalytic properties. Moreover, the TiO_2 coating on a low cost and industry friendly substrate like stainless steel (SS) is highly required for medical applications.

In this letter, we demonstrate the effectiveness of OFR in achieving desired crystalline phases of reduced-TiO_2 films on SS substrates by radio frequency (RF) magnetron sputtering at RT. The transformation of anatase to rutile through intermediate mixed phases as a function of OFR is observed and discussed on the basis of X-ray diffraction (XRD) with Rietveld refinement and X-ray absorption spectroscopy (XAS) analyses. We also show the reduction of the optical bandgap by lowering OFR during deposition and simultaneous appearance of sub-bandgap states. Finally, improved photocatalytic degradation of methylene blue (MB) aqueous solution has been demonstrated in the presence of mixed phases of TiO_2 films.

Here, TiO_2 thin films of ~100 nm thickness were deposited on SS substrates by varying OFR from 0 to 20 sccm in a RF magnetron sputtering system (Excel Instruments, India).

a)Author to whom correspondence should be addressed: aloke.kanjilal@snu.edu.in

A commercially purchased TiO_2 target (from MTI, USA) was used for thin film deposition. Argon gas was purged at 30 sccm in all depositions, while RF power was maintained at 100 W. A substrate rotation of 9-rpm was kept for uniform deposition. The base and working pressures of the deposition system were 5×10^{-7} and 8 mTorr, respectively. The SS substrates were ultrasonicated in acetone, isopropyl alcohol (IPA), and water for 10 min each before deposition. The crystallinity of the as-deposited films was investigated in coupled θ-2θ diffraction (Bruker D8 discover) using Cu-K_α radiation. The optical bandgap was measured in the diffuse reflectance mode by using an integrating sphere of the UV-Vis-NIR spectrophotometer (Shimadzu Solid Spec-3700). Moreover, XPS measurements were carried out in an Omicron EA-125 photoelectron spectrometer at RRCAT, India, with an Al K_α radiation (energy 1486.6 eV). However, the local disorder, a decisive factor in bandgap tuning, was studied by XAS at the soft *X*-ray absorption beamline (BL-1) of Indus-2 synchrotron radiation facility with a storage ring operated at 2.5 GeV at RRCAT.[16] Finally, the photocatalytic activity of the as-prepared thin films towards the degradation of MB in de-ionised water was studied under ultraviolet (UV) radiation. A medium pressure 450 W mercury lamp radiating in the spectral range of 200–400 nm with predominant peaks at 254, 356, and 365 nm was used for ultra-violet radiation. Post-irradiation samples were collected at regular intervals of 30 minutes for recording the UV-Vis spectra for degradation studies.

Figure 1 shows the GIXRD patterns with Rietveld analyses[17,18] of TiO_2 films prepared with 0 (S0), 6 (S6), 12 (S12), and 20 sccm (S20) OFR at a constant working pressure of 8 mTorr. The XRD data reveal a drastic change from the anatase to rutile dominated crystalline phase with increasing OFR. The extracted values of lattice parameters, crystallite size, microstrain, and relative phase abundances of anatase and rutile from the Rietveld's refined outputs are summarized in Table S1 (supplementary material). As expected, only the anatase phase is present in S0, but both anatase and rutile phases exist in other three samples with different contents. With increasing OFR, rutile phase contribution is more dominated. The change in phase contribution with the OFR is depicted in Fig. S1. It is clear that the volume fraction of anatase and rutile phases is 62.95% and 38.05%, respectively, in S6, whereas that of the corresponding phases are eventually 34.20% and 65.80%, respectively, in S12.

To understand the change in chemical states of Ti, detailed XPS measurements have been performed at the Ti-2*p* edge. The change in the Ti-2*p* spectrum with increasing OFR in S0, S6, S12, and S20 is presented in Fig. 2, showing a clear variation in shapes of the Ti $2p_{3/2}$ and $2p_{1/2}$ peaks. For in-depth understanding, the Ti-2*p* peak was deconvoluted in a standard Computer Aided Surface Analysis for XPS (CASA-XPS) processing software using *Voigt-function*. The extracted binding energy (BE) and atomic concentration corresponding to Ti^{4+}, Ti^{3+}, and Ti^{2+} states are tabulated in Table S2. In S0, the peak fitting of Ti-2*p* indicates the presence of TiO_2 (Ti^{4+} at 459.2/464.7 eV)[19] with two shoulder peaks at low BE for oxygen-deficient Ti_2O_3 (Ti^{3+} at 457.6/462.65 eV)[20] and TiO (Ti^{2+} at 456.6/460.4 eV)[21] phases. A significant amount (~39%) of $Ti^{3+/2+}$ states have been observed in S0, where the intermediate $Ti^{3+/2+}$ states start decreasing with increasing OFR. The intermediate $Ti^{3+/2+}$ states in S6 and S12 samples reach atomic concentrations of 35% and 26%, respectively. Interestingly, these two phases completely disappeared with a further increase in OFR (i.e., S20), and the spectrum corresponds to the stoichiometric TiO_2 phase. XPS analysis, therefore, provides a clear evidence of transformation from the sub-stoichiometric to stoichiometric TiO_2 (Ti^{4+}) phase with increasing OFR and that eventually changes the crystallinity of the samples as observed in XRD patterns (Fig. 1).

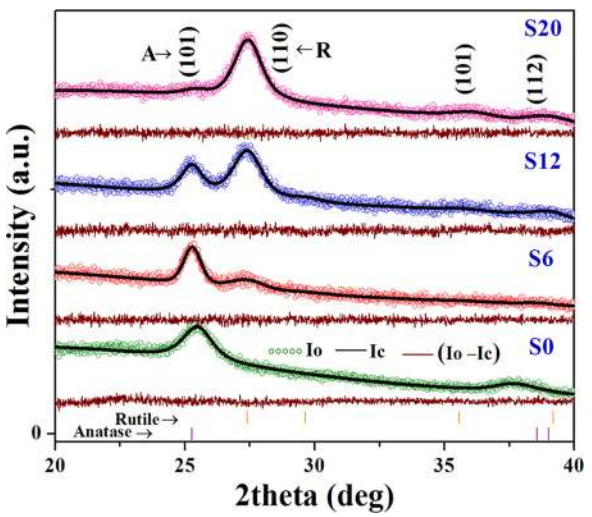

FIG. 1. Typical Rietveld analysis of the GIXRD fitted patterns of all compounds, where the experimental (I_O) data are shown as hollow spheres (o) and simulated patterns (I_C) are shown by solid lines; here, ($I_O - I_C$) represents the corresponding difference of each pattern.

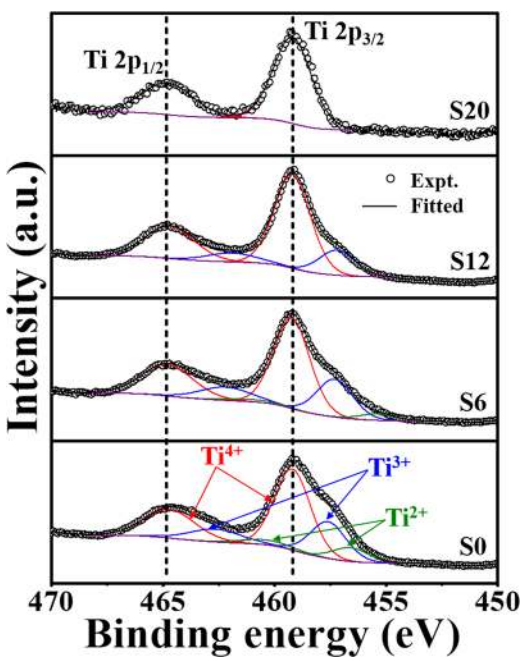

FIG. 2. High resolution XPS spectra of Ti 2*p* ($2p_{1/2}$ and $2p_{3/2}$) states for S0, S6, S12, and S20 samples are exhibited, showing a gradual decrease in deconvoluted oxidation states from a coexistence of $Ti^{2+/3+/4+}$ (S0) to only Ti^{4+} (S20) with an increase in OFR from 0 to 20 sccm.

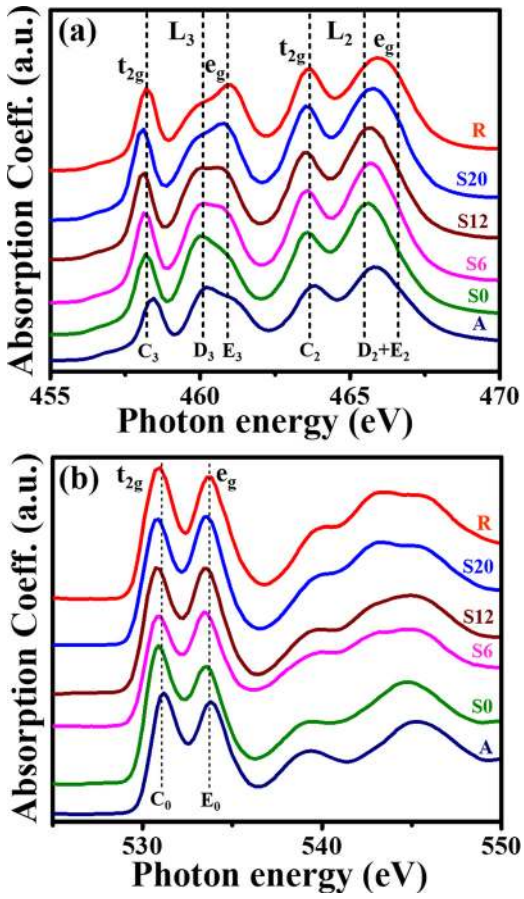

FIG. 3. XAS spectra of (a) Ti *L*-edge and (b) O *K*-edge for standard anatase (*A*), S0, S6, S12, and S20 samples and also for standard rutile (*R*).

To get an insight of the local electronic configuration of the constituent atoms of TiO_{2-x}, the as-prepared samples have been characterized by XAS. The Ti *L*-edge is shown in Fig. 3(a), reflecting the transitions of Ti-2*p* core electrons to Ti-3*d* states in the conduction band.[22] Due to spin-orbit coupling of Ti-2*p* electrons, the Ti *L*-edges of S0, S6, S12, and S20 are split into two main components L_2 and L_3, separated by ~5.5 eV.[22,23] The characteristics of L_2 were found to be broadened with respect to L_3 owing to the shorter lifetime of its excited state ($2p_{1/2}$ core hole) as a consequence of a radiation-less transition of electrons from $2p_{3/2}$ to $2p_{1/2}$ levels, associated with the furtherance of a valence electron to the conduction band.[23,24] Moreover, the crystal-field of surrounding O-atoms splits the Ti-3*d* state into two sub-levels, t_{2g} and e_g,[24] where the Ti e_g level (consisting of $d_{x^2-y^2}$ and d_{z^2} orbitals) is very sensitive to the local bonding, and so, it gives a relatively large broadening compared to t_{2g}. This is because of the involvement of Ti-e_g orbits directed towards the surrounding O-2*p* in a larger degree of hybridization.[22] Moreover, a clear splitting of e_g contribution of the L_3 edge into two more peaks (denoted as D_3 and E_3) is clearly visible in Fig. 3(a). A similar splitting of the e_g band (into D_2 and E_2 peaks) also exists for the L_2 edge but not well resolved owing to the short lifetime of $2p_{1/2}$ as stated above. It is seen from Fig. 3(a) that the D_2 and D_3 peak intensities are reduced with increasing OFR, while the E_2 and E_3 peaks of the e_g band for both L_2 and L_3 edges are dominating. Close inspection reveals that with varying OFR, the $D_2 + E_2$ peaks are slightly shifted towards higher energy. This results in an overall shift of the broad e_g peak of L_2 to higher energy signifying an increase in a long range order of the TiO_2 films.[22] The variation of the relative intensities of D_3 and E_3 peaks comprises different degrees of octahedral symmetry corresponding to anatase and rutile phases of TiO_2.[24] Interestingly, the D_3/E_3 intensity ratio for S20 and S0 matches well with that for the standard rutile and anatase phases, respectively, confirming their phase dominance. In the case of S6 and S12, a gradual increase in E_3 peak intensity is clearly observed. Thus, spectra of S0 to S20 show a significant evolution of E_3 peaks as a function of OFR which depicts a dominating rutile phase. This is also confirmed from the decreasing trend of the intensity ratio of D_3/E_3 with increasing OFR as tabulated in Table I. The results conclude the dominance of the rutile phase at higher OFR which is consistent with the XRD results.

The O-*K* edge spectra were also investigated for further understanding of local stoichiometry and oxidation states. The recorded O-*K* edge spectra in Fig. 3(b) show C_0 and E_0 peaking at ~531 and 534 eV with additional structures at higher energies. Similar to Ti $L_{2,3}$-edge XAS, the O *K*-edge also reflects the unoccupied electronic structure of the Ti ions that are bound with O-2*p* orbitals through the O-2*p* to Ti-3*d* (or 4*sp*) orbital hybridizations. The first two intense peaks at an energy of 530–535 eV for each of the spectra are associated with the transition from O-2*p* to Ti-3*d* states.[25] The appearance of two peaks t_{2g} and e_g is due to the crystal-field splitting, where the peak intensity might change depending on their local structures.[24] Since the e_g peak is sensitive to the local structure than the t_{2g} peak, the increasing trend in intensity of the former one signifies a gradual rise in long-range order with increasing OFR. The peaks in the energy range of 537–548 eV represent the unoccupied Ti-4*sp* states, where the peak intensities in S0 are found to be intensified with increasing OFR. This emergence of distinct peaks signifies the presence of a long range order.

TABLE I. X-ray absorption spectroscopy profiles recorded at Ti *L* and O *K*-edges for S0, S6, S12, and S20 along with standard anatase and rutile are tabulated. The peaks at the Ti *L*-edge are levelled by C_2, D_2, E_2, C_3, D_3, and E_3 while O *K*-edge peaks are levelled by C_0 and E_0.

Sample	C_3 (eV)	D_3 (eV)	E_3 (eV)	C_2 (eV)	D_2 (eV)	D_3/E_3	C_3/D_3	C_2/D_2	C_O (eV)	E_O (eV)
Rutile (R)	458.2	460.0	460.9	463.6	465.9	0.93	1.06	0.95	531.0	533.7
S20	458.1	459.9	460.7	463.5	465.8	0.94	1.03	0.92	530.9	533.5
S12	458.1	459.8	460.7	463.5	465.6	0.99	0.97	0.89	530.8	533.5
S6	458.1	459.8	460.9	463.6	465.6	1.02	0.94	0.87	530.9	533.5
S0	458.1	459.9	460.9	463.6	465.6	1.13	0.88	0.83	530.9	533.5
Anatase (A)	458.4	460.1	461.2	463.8	465.8	1.15	0.91	0.87	531.2	533.8

In order to monitor the change in the optical bandgap of the TiO_2 films as a function of increasing OFR, UV-Vis spectroscopy has been recorded in the diffuse reflectance (R_D) mode and analysed the results by Kubelka–Munk (K-M) function $F(R_D) = \frac{P(1-R_D)^2}{2R_D}$.[14] The relationship between the K-M function and the bandgap energy (E_g) for indirect bandgap TiO_2 can be described by the following equation: $\frac{F(R_D)h\upsilon}{t} = P(h\upsilon - E_g)^2$, where P is a constant and t is the layer thickness. The impact of increasing OFR in tuning the optical bandgap of TiO_2 thin films is shown in Fig. 4. As expected, the bandgap is increased from 2.65 eV (S6) to 3.22 eV (S20) with increasing OFR. Since the conduction-band (CB) and valence-band (VB) of TiO_2 are associated with the Ti-3*d* and O-2*p* levels, respectively, any rearrangement of Ti and O-atoms can bring a change in BEs of Ti-3*d* and O-2*p* states and as a result modify the optical bandgap of TiO_2.[26] Therefore, the low bandgap of S6 and S12 as compared with S20 could be attributed to the presence of Ti^{3+} which can take part in creating sub-bandgap states by breaking bonds of TiO_2.[14,27] This is consistent with XPS analysis, showing an increase in concentrations of Ti^{3+} with decreasing OFR during deposition. However, S0 showed a Fabry-Perot oscillation owing to multiple reflection and resonance of the reflecting wavelengths from the sharp SS/TiO_2/air interfaces.[28]

The relevance of TiO_2 films was weighed by degradation of aqueous MB solution under UV irradiation. Following the addition of the photocatalyst in the dark condition for initial 30 min, merely any degradation of MB was noticed, while after irradiation for 330 min, dye was almost degraded. The dependencies of C_t/C_0 with irradiation time are plotted in Fig. 5, whereas the rate constant k was determined for each sample from the slope of $\ln(C_0/C_t)$ vs irradiation time (using pseudo-first-order kinetic equation) plot in Fig. S2, where C_0 and C_t represent the concentrations of MB solution before and after irradiation, respectively. The best catalytic performance can be seen for S12 (98.3%) with $k = 11.92 \times 10^{-3}\,\text{min}^{-1}$, followed by S6 (94.8%, $k = 8.74 \times 10^{-3}\,\text{min}^{-1}$), S20 (94.13%, $k = 8.05 \times 10^{-3}\,\text{min}^{-1}$), and S0 (91.8%, $k = 7.34 \times 10^{-3}\,\text{min}^{-1}$), though S0 shows a fast degradation compared to S20 up to 300 min. The catalytic efficiency of S12 has further been compared with

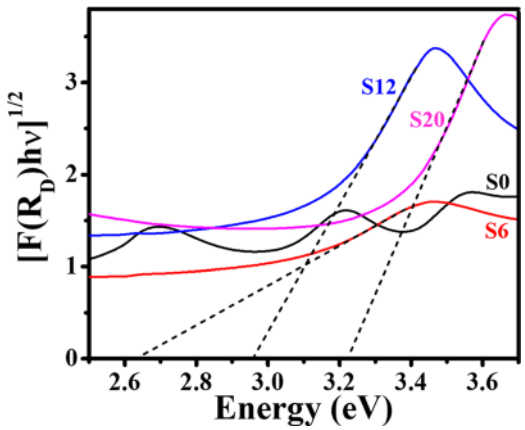

FIG. 4. Plots of the transformed Kubelka-Munk function $[(F(R_D)h\upsilon)^{1/2}]$ versus incident photon energy ($h\upsilon$) for the S0, S6, S12, and S20 samples show a decreasing trend of the energy bandgap with decreasing OFR.

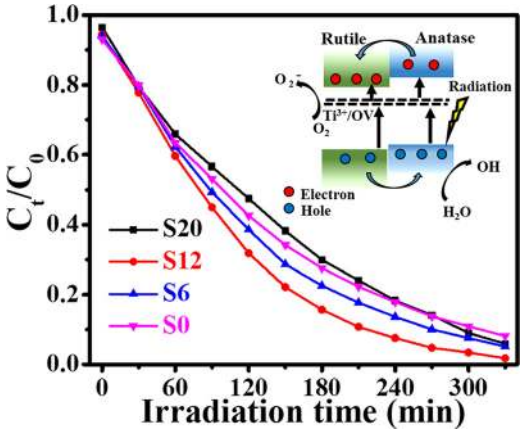

FIG. 5. Photocatalytic degradation of Methylene Blue under UV radiation for different TiO_2 samples grown at varying OFR (inset: schematic diagram of photocatalytic charge transportation in anatase-rutile mixed phase TiO_2 for S12).

commercially available P25 (anatase + rutile), as documented in the supplementary material (Fig. S3), showing the superior behaviour of the former one.

It is commonly believed that the anatase dominated TiO_2 provides better catalytic activity than rutile.[29] However, the present finding gives a much slower degradation of MB in S0 consisting of anatase crystallites only (Fig. 1). This could be due to the fact that the dominance of Ti^{2+} in the Ti^{2+}/Ti^{3+} driven deep level states (Fig. 2) may enhance the trapping of photogenerated carriers and in turn decrease the photocatalytic activity of S0.[30,31] The increase in catalytic activity via reduction of the relative contribution of Ti^{2+} in S6 also supports this claim. On the other hand, the decrease in catalytic performance in S20 is possibly due to the emergence of the rutile structure which itself has a high charge recombination rate.[32] In fact, the highest photodegradation in S12 (in the absence of Ti^{2+}) consisting of both anatase and rutile phases is due to the intergranular charge transfer process,[15] where the creation of Ti^{3+} (Fig. 2) is accompanied by generation of OVs owing to charge neutrality. These self doped Ti^{3+} and/or OVs together will create localized states near CB minima of reduced TiO_2 which in turn results in bandgap narrowing.[33] Therefore, under the UV exposure, electrons from the VB are excited to these localized states first and then from there to the CB. As the electron affinity of rutile is higher than that of anatase, a type-II staggered band structure is formed between their vicinal contact points[26] which assists a smooth flow of charge carriers (photogenerated conduction electrons) from anatase to rutile phases. Similarly, the holes are accumulated in the VB of anatase from rutile owing to their relative VB positions. This charge transfer hinders the e-h pair recombination and increases their lifetime. These photo-generated electrons migrate to the photocatalyst surface and take part in formation of $\cdot O_2^-$ and other oxidative species by capturing the molecular oxygen in solution. Meanwhile, the accumulated holes on the surface of reduced TiO_2 directly take part in photocatalysis and degrade the MB. As a result, it is proposed that the mixed *A*- and *R*-TiO_2 phases enhance the photocatalytic activity in S12 and the expected mechanism is projected in the inset of Fig. 5.

In conclusion, the growth of TiO_2 films on SS by RF magnetron sputtering under controlled OFR was demonstrated,

showing a systematic formation of oxygen-deficient Ti_2O_3 and TiO phases with a reduced bandgap. A control over anatase and rutile phases was illustrated by simply varying the OFR at RT at constant chamber pressure and manifested by XRD analyses. The presence of a long-range order besides transformation from *A*-TiO_2 to *R*-TiO_2 at higher OFR was further detected by XAS measurements. Eventually, an enhanced photodegradation of MB was monitored in S12 owing to the presence of mixed phases, supported by the near surface type-II staggered band structure for smooth flow of photogenerated electrons from anatase to rutile structures.

See supplementary material for (1) specifications of Rietveld refinement of the obtained GIXRD patterns, (2) Table S1: structural parameters obtained from the Rietveld analysis of TiO_2, (3) Table S2: XPS results of TiO_2 grown at different oxygen flow rates, (4) $\ln(C_0/C_t)$ vs irradiation time plot for methylene blue, and (5) comparison of photocatalytic performance of S12 with P25.

The authors would like to acknowledge the help received from beamline scientists, especially staff Mr. Rakesh Sah for XAS measurements in the BL-1 beamline of Indus-2 at RRCAT, Indore. The authors would like to acknowledge the financial support received from Shiv Nadar University and also from Department of Science and Technology India under Project No. DST/EMR/2014/000971.

[1]E. Bet-Moushoul, Y. Mansourpanah, K. Farhadi, and M. Tabatabaei, Chem. Eng. J. **283**, 29 (2016).
[2]D. Macwan, P. N. Dave, and S. Chaturvedi, J. Mater. Sci. **46**, 3669 (2011).
[3]S. Goswami, A. J. Matula, S. P. Rath, S. Hedström, S. Saha, M. Annamalai, D. Sengupta, A. Patra, S. Ghosh, and H. Jani, Nat. Mater. **16**, 1216 (2017).
[4]M. Ni, M. K. Leung, D. Y. Leung, and K. Sumathy, Renewable Sustainable Energy Rev. **11**, 401 (2007).
[5]S. C. Pillai, P. Periyat, R. George, D. E. McCormack, M. K. Seery, H. Hayden, J. Colreavy, D. Corr, and S. J. Hinder, J. Phys. Chem. C **111**, 1605 (2007).
[6]U. Akpan and B. Hameed, J. Hazard. Mater. **170**, 520 (2009).
[7]A. Naldoni, M. Allieta, S. Santangelo, M. Marelli, F. Fabbri, S. Cappelli, C. L. Bianchi, R. Psaro, and V. Dal Santo, J. Am. Chem. Soc. **134**, 7600 (2012).
[8]D. Rafieian, W. Ogieglo, T. Savenije, and R. G. Lammertink, AIP Adv. **5**, 097168 (2015).
[9]A. Gautam, A. Kshirsagar, R. Biswas, S. Banerjee, and P. K. Khanna, RSC Adv. **6**, 2746 (2016).
[10]J. Zhang, P. Zhou, J. Liu, and J. Yu, Phys. Chem. Chem. Phys. **16**, 20382 (2014).
[11]J. C. Yu, J. Yu, W. Ho, Z. Jiang, and L. Zhang, Chem. Mater. **14**, 3808 (2002).
[12]Z. Wang, B. Wen, Q. Hao, L.-M. Liu, C. Zhou, X. Mao, X. Lang, W.-J. Yin, D. Dai, and A. Selloni, J. Am. Chem. Soc. **137**, 9146 (2015).
[13]B. Choudhury and A. Choudhury, Physica E **56**, 364 (2014).
[14]C. P. Saini, A. Barman, B. Satpati, S. Bhattacharyya, D. Kanjilal, and A. Kanjilal, Appl. Phys. Lett. **108**, 011907 (2016).
[15]T. Van der Meulen, A. Mattson, and L. Österlund, J. Catal. **251**, 131 (2007).
[16]D. M. Phase, M. Gupta, S. Potdar, L. Behera, R. Sah, and A. Gupta, AIP Conf. Proc. **1591**, 685 (2014).
[17]H. Rietveld, Acta Crystallogr. **22**, 151 (1967).
[18]S. Bid and S. Pradhan, J. Appl. Crystallogr. **35**, 517 (2002).
[19]M. Wagstaffe, H. Hussain, M. J. Acres, R. Jones, K. L. Syres, and A. G. Thomas, J. Phys. Chem. C **121**, 21383 (2017).
[20]Y. Liu, J. Wang, P. Yang, and K. Matras-Postolek, RSC Adv. **5**, 61657 (2015).
[21]E. McCafferty and J. Wightman, Appl. Surf. Sci. **143**, 92 (1999).
[22]S. O. Kucheyev, T. van Buuren, T. F. Baumann, J. H. Satcher, T. M. Willey, R. W. Meulenberg, T. E. Felter, J. F. Poco, S. A. Gammon, and L. J. Terminello, Phys Rev. B **69**, 245102 (2004).
[23]J. Crocombette and F. Jollet, J. Phys.: Condens. Matter **6**, 10811 (1994).
[24]G. Van Der Laan, Phys. Rev. B **41**, 12366 (1990).
[25]S. J. Stewart, M. Fernández-García, C. Belver, B. S. Mun, and F. G. Requejo, J. Phys. Chem. B **110**, 16482 (2006).
[26]D. O. Scanlon, C. W. Dunnill, J. Buckeridge, S. A. Shevlin, A. J. Logsdail, S. M. Woodley, C. R. A. Catlow, M. J. Powell, R. G. Palgrave, and I. P. Parkin, Nat. Mater. **12**, 798 (2013).
[27]Z. Pei, L. Ding, H. Lin, S. Weng, Z. Zheng, Y. Hou, and P. Liu, J. Mater. Chem. A **1**, 10099 (2013).
[28]T. Abhilash, M. Balasubrahmaniyam, A. Patra, and S. Kasiviswanathan, Appl. Phys. Lett. **104**, 241112 (2014).
[29]G. Odling and N. Robertson, ChemSusChem **8**, 1838 (2015).
[30]K. Eufinger, D. Poelman, H. Poelman, R. De Gryse, and G. Marin, *Thin Solid Films: Process and Applications* (Transworld Research Network, 2009), p. 189.
[31]M. Zare, A. Mortezaali, and A. Shafiekhani, J. Phys. Chem. C **120**, 9017 (2016).
[32]M. Sachs, E. Pastor, A. Kafizas, and J. R. Durrant, J. Phys. Chem. Lett. **7**, 3742 (2016).
[33]Y. Shiraishi, Y. Togawa, D. Tsukamoto, S. Tanaka, and T. Hirai, ACS Catal. **2**, 2475 (2012).